SCIENCE CHINA
Information Sciences

• RESEARCH PAPER •

April 2025, Vol. 68, Iss. 4, 140404:1–140404:11
https://doi.org/10.1007/s11432-024-4178-x

Special Topic: Photonics Technology

Temporal-spectral correlation dynamics of Raman random fiber laser

Longqun NI[1†], Yifei QI[1†], Xingyu BAO[1], Jing ZHANG[1], Pan WANG[1], Han WU[2] & Zinan WANG[1*]

[1]*Key Laboratory of Optical Fiber Sensing and Communications, University of Electronic Science and Technology of China, Chengdu 611731, China*
[2]*College of Electronics and Information Engineering Sichuan University, Chengdu 610064, China*

Received 7 June 2024/Revised 27 July 2024/Accepted 24 August 2024/Published online 7 March 2025

Abstract Raman random fiber laser (RRFL) possesses rich physical properties of spectral, temporal, and spatial domains due to its unique feedback mechanism and complex nonlinear effects. Characterizing and controlling the microscopic evolution dynamics of RRFL are crucial to driving breakthrough advances in fields such as inertial confinement fusion and fundamental physics. In this work, a novel experimental and theoretical analysis of the evolution of the temporal spectral correlations of the RRFL in the transition and steady states is conducted. In the transitional state, the microscopic dynamics of the RRFL excitation process is revealed comprehensively: the temporal-correlation growth curve contrasts with that of resonant-cavity lasers, and the formation and degradation of spectral correlation are observed. In the steady state, the overall spectrum is characterized by partial correlation, and the correlation characteristics of RRFL mainly originate from the spectral random spikes, which offers a novel dimension for the precise control of RRFL correlation. This work provides new insights into underlying physical properties of continuous broadband lasers, offering key guidance for laser design, control, and applications.

Keywords random fiber laser, microscopic characteristics, temporal-spectral correlation, random spikes, nonlinear optics

Citation Ni L Q, Qi Y F, Bao X Y, et al. Temporal-spectral correlation dynamics of Raman random fiber laser. Sci China Inf Sci, 2025, 68(4): 140404, https://doi.org/10.1007/s11432-024-4178-x

1 Introduction

Raman random fiber laser (RRFL) is a novel light source [1–4] and the feedback is derived from randomly distributed Rayleigh scattering [5] caused by microstructural irregularities in the fiber [6, 7]. The unique feedback mechanism and 1D geometry endow RRFL with inherent directionality [8], overcoming the drawbacks of conventional random lasers while preserving the advantages of their low cost and simple fabrication [9, 10]. Due to its distinctive optical characteristics [11, 12], such as high efficiency [13], low coherence [14], and modeless emission [15], RRFL has been widely used in optical communications [2], speckle-free imaging [16], and fiber sensing [17], and is expected to be a high-power laser device seed source for the next-generation inertial confinement fusion (ICF) experiments [18]. Benefiting from the unique disorder and randomness of Rayleigh scattering as well as the interaction of multiple nonlinear effects, RRFL contains rich physical properties in the spectral, temporal, and spatial domains [19, 20], making it an ideal platform for understanding and exploring complex physical systems, which has sparked significant interest in the research community to study the fundamental physics of laser radiation.

In this context, the steady state characteristics of RRFL have been extensively researched. In the spectral domain, Sugavanam et al. [21] utilized a scanning Fabry-Perot interferometer for real-time spectral measurements of RRFL, unveiling long-lived narrow spectral components in the RRFL's spectrum and their dynamic properties. Moreover, through mutual information analysis, nonlinear correlations between the different wavelength intensities were revealed. Subsequently, Li et al. [22] conducted an in-depth analysis of the statistical characteristics of spectral intensity fluctuations, revealing a universal pattern: statistical evolution from a Gaussian to a Lévy and then back to a Gaussian distribution, which further deepened the understanding of the nature of excitation physics in RRFL. In addition, unique

* Corresponding author (email: znwang@uestc.edu.cn)
† These authors contributed equally to this work.

Table 1 Review the main historical development of RRFL correlation.

Year	Key finding	Method	Laser state
2015 [26]	Temporal PDF deviates from Gaussian distribution	Direct detection	Steady state
2017 [21]	Observe narrowband components and analyze their correlations	FPI	Steady state
2019 [22]	Spectral PDF transitions from Gaussian distribution to Lévy distribution and then back to Gaussian distribution at different pump powers	Spectral filtering	Steady state
2019 [20]	Analyze the interactions of spectral components in multi-wavelength radiation and identify where they occur	Multi-channel simultaneous measurement	Steady state
2021 [32]	Introduce a modified Pearson coefficient to analyze correlation evolution and the RSB phenomenon in electronically addressable RFL	Direct detection	Steady state
2021 [27]	Full-bandwidth characterization of temporal PDF for different spectral parts	Spectral filtering	Steady state
2024 [31]	Investigate the build-up and dissipation processes of lasers and track the temporal and spectral evolution	Time-slicing method	Transitional state

phase transition phenomena marked by replica symmetry breaking (RSB) were observed on the RRFL platform [23–25], further revealing the intricate spectral properties inside RRFL. In the time domain, Gorbunov and collaborators [26] experimentally investigated the temporal characteristics and intensity dynamics of RRFL and found that the statistical properties deviate from a Gaussian. Further utilizing the optical filtering method, the intensity statistics of different spectral components was measured [27]. Besides, many complex physical theories, e.g., the optical rogue waves [28, 29] and turbulent behavior [30], were observed in the RRFL. However, these researches mainly focus on the measurement and statistical analysis of macroscopic parameters, lacking the characterization of RRFL microscopic dynamic properties.

In addition to the steady-state properties, the evolutionary dynamics of the transition state is also crucial for understanding the physical implications of RRFL. However, the study of transition state dynamics remains in the preliminary stage due to the inherent continuous broadband nature of RRFL. To overcome this challenge, Lin et al. [31] utilized a time-slicing method to investigate the build-up and dissipation processes of RRFL. The build-up of RRFL showed continuous Verhulst logistic growth curves and the spectral evolution underwent two stages, from spectral density increase to spectral broadening. This work offered a new perspective on comprehending the fundamental physics of random lasing. However, limited by the spectral measurement speed, only in the order of Hz, the time-slicing method can only measure the laser characteristics within a specific sliced time, and the complete evolution dynamics of RRFL in transitional states has not been studied. Table 1 [20–22,26,27,31,32] reviews the main historical development of RRFL correlation research.

In this paper, the entire evolution process of the RRFL is directly observed and investigated both experimentally and theoretically. In the transitional state, the temporal correlation increases continuously and finally converges to a stable value, and these evolutionary characteristics depend on the feedback mechanism. In contrast, the evolution of spectral correlation shows the same pattern: firstly, the central wavelength spectrum exhibits high spectral correlation due to the gain competition and gain sharing; subsequently, as the accumulation of pump energy, the wavelengths on both sides begin to radiate and exhibit high correlation, and the correlation of center wavelength begins to degrade simultaneously. In the steady state, the overall spectrum features partial correlation in the spectral domain, and the temporal-spectral correlation characteristics are mainly driven by random spikes. This unique property provides novel methods for controlling the correlation of the RRFL. Our investigations comprehensively reveal the complex dynamic evolution of RRFL, providing important guidance for better design, tailoring, and optimization of lasers.

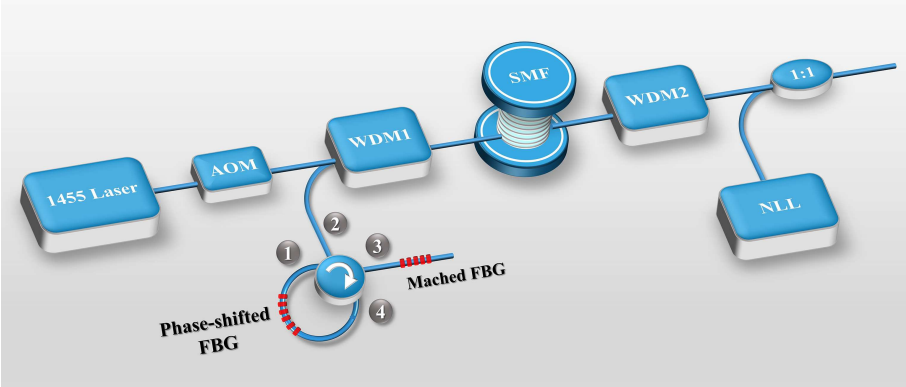

Figure 1 (Color online) Experimental setup for investigating the evolution dynamics of Raman random fiber laser. AOM: acoustic optic modulator; WDM: wavelength division multiplexer; SMF: single mode fiber; NLL: narrow linewidth tunable laser.

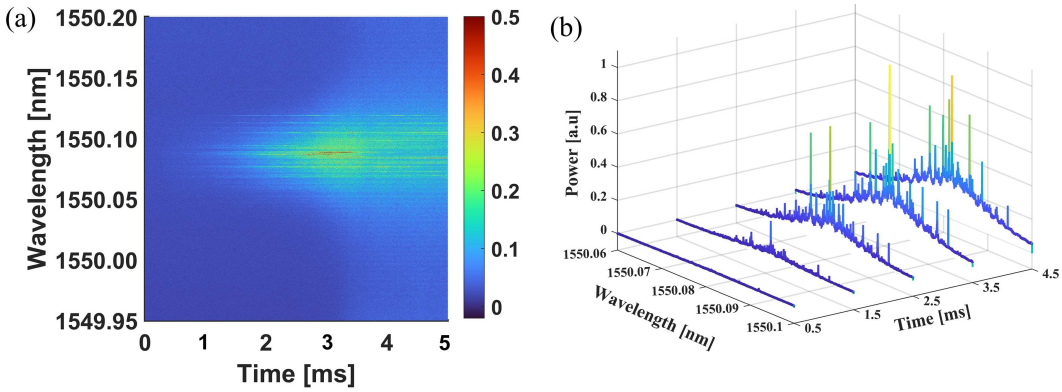

Figure 2 (Color online) (a) Temporal spectrogram using the beat-frequency operation. The entire process of transition from amplified spontaneous emission noise to random laser radiation can be clearly observed. (b) Evolution of the emission spectrum as a function of RRFL build-up time.

2 Methods

2.1 Experiment setup

The Raman random fiber laser used in the experiment is of a forward-pumped, grating-based, narrowband configuration, using stimulated Raman scattering (SRS) for gain and employing 50 km single mode fiber (SMF) for generating the randomly distributed feedback, as illustrated in Figure 1. The RRFL is pumped by a 1455 nm laser and each transition of the pump from OFF to ON state is controlled by an acoustic-optic modulator (AOM). The output pump is injected into the laser cavity via a 1455 nm/1550 nm wavelength division multiplexer (WDM), and the 1550 nm port is connected to a 1550 nm phase-shift fiber Bragg grating (FBG), which utilizes 0.02 nm transmission peak to provide point feedback to meet the bandwidth of the detector and oscilloscope. The generated RRFL is separated from the pump by an additional 1455 nm/1550 nm WDM. To achieve rapid and high-precision spectral detection, a narrow linewidth tunable laser (NLL) is used in combination with the generated RRFL for beat-frequency operation in the experiment [33, 34]. The 5 ms data stream is detected by a 40 GHz photoreceiver and sampled by an oscilloscope (OSC) at a 40 GSa/s sampling rate. By performing a short-time Fourier transform on the time signals, the temporal-frequency domain information of the RRFL can be extracted. The temporal and frequency resolutions in this work are 1 μs and 2 MHz, respectively. The RRFL has a 3 dB bandwidth of 2.5 GHz, so it can cover the entire evolution of RRFL, i.e., from the amplified spontaneous emission noise to stable random lasing.

In order to validate the feasibility of the beat-frequency operation in rapidly measuring real-time spectra of RRFL. The evolution of spectra can be obtained by doing a short-time Fourier transform (STFT) of temporal domain data, as depicted in Figure 2(a), which contains 10000 individual spectra. The entire process of transition from amplified spontaneous emission noise to random laser radiation can be observed. In more detail, Figure 2(b) illustrates the spectral evolution of RRFL in different

Table 2 Parameters set in the simulation.

Parameter	Pump	Stoke
λ	1455 nm	1550 nm
v_{gs}	2.0504×10^8 m/s	2.0497×10^8 m/s
α	0.24 dB/km	0.2 dB/km
g	4.14×10^{-4} m$^{-1} \cdot$ W^{-1}	–
γ	0.0017 m$^{-1} \cdot$ W^{-1}	0.0014 m$^{-1} \cdot$ W^{-1}
$\overline{\varepsilon}$	0.6×10^{-7} m^{-1}	0.45×10^{-7} m^{-1}
β_2	-1.7324×10^{-26} s^2/m	-2.7927×10^{-26} s^2/m
R_L	4×10^{-5}	0.99
R_R	4×10^{-5}	4×10^{-5}

transitional states. At the 1.5 ms moment, the RRFL starts to build up and shows a few random spikes in the spectrum; as the laser tends to the steady state, the number of random spikes in the spectrum gradually increases, and the spectrum pedestal becomes wider and higher. These results indicate that the beat-frequency operation can accurately capture spectral information, which provides an efficient way to study the dynamic evolution of RRFL.

2.2 Simulation model

Before the experiment, we also performed simulations to theoretically analyze the RRFL dynamic evolution properties. The simulation model is based on the generalized nonlinear Schrödinger equations (NLSEs) that can describe the spectral and temporal dynamics of RRFL [3, 35, 36]:

$$\frac{\partial u_p^{\pm}}{\partial z} \mp \frac{1}{v_{gs}} \frac{\partial u_p^{\pm}}{\partial t} \pm \mathrm{i}\frac{\beta_{2p}}{2} \frac{\partial^2 u_p^{\pm}}{\partial t^2} \pm \frac{\alpha_p}{2} u_p^{\pm} = \pm \mathrm{i}\gamma_p \left|u_p^{\pm}\right|^2 u_p^{\pm} \mp \frac{g_p(\omega)}{2} \left(\left\langle \left| u_s^{\pm} \right|^2 \right\rangle + \left\langle \left| u_s^{\mp} \right|^2 \right\rangle \right) u_p^{\pm}, \tag{1}$$

$$\frac{\partial u_s^{\pm}}{\partial z} \pm \mathrm{i}\frac{\beta_{2s}}{2} \frac{\partial^2 u_s^{\pm}}{\partial t^2} \pm \frac{\alpha_s}{2} u_s^{\pm} \mp \frac{\varepsilon(\omega)}{2} u_s^{\mp} = \pm \mathrm{i}\gamma_s \left|u_s^{\pm}\right|^2 u_s^{\pm} \pm \frac{g_s(\omega)}{2} \left(\left\langle \left| u_p^{\pm} \right|^2 \right\rangle + \left\langle \left| u_p^{\mp} \right|^2 \right\rangle \right) u_s^{\pm}. \tag{2}$$

The left-hand sides of (1) and (2) describe the linear processes in the optical fiber, including dispersion, attenuation, and Rayleigh scattering. The right-hand sides describe the nonlinear processes in the optical fiber, where $\mathrm{i}\gamma \left|u^{\pm}\right|^2 u^{\pm}$ represents the self-phase modulation process and $\frac{g(\omega)}{2}(\langle |u^{\pm}|^2 \rangle + \langle |u^{\mp}|^2 \rangle) u^{\pm}$ represents the Raman scattering effect. Specifically, u is the complex field envelope, t is the time in a frame of reference moving with the pump, and v_{gs} denotes the group velocities difference between pump and Stokes waves. α, γ, β_2, g are the linear fiber loss, Kerr coefficient, second-order dispersion, and Raman gain, respectively; ε is Rayleigh scattering, whose intensity and phase are related to frequency and time [3]. Sign "$\mp$" denotes counter-propagating waves; p and s are used for pump and Stokes waves; ω is the angular frequency of light waves.

In addition, the boundary conditions can be described as

$$P_p^+(0,\omega,t) = P_{\mathrm{in}}(\omega) T_{L_P} + R_{L_p}(\omega) P_p^-(0,\omega,t),\ P_p^-(L,\omega,t) = R_{\mathrm{R}_P}(\omega) P_p^+(\mathrm{L},\omega,t), \tag{3}$$

$$P_s^+(0,\omega,t) = R_{L_s}(\omega) P_s^-(0,\omega,t),\ P_s^-(L,\omega,t) = R_{R_s}(\omega) P_s^+(L,\omega,t), \tag{4}$$

where $R_L(\omega)$ and $R_R(\omega)$ are the reflectivity of the FBG and the fiber end, respectively, and R_L denotes the corresponding transmittance. P_{in} is the input pump power and the fiber length is defined as L. T_{L_p} is the transmittance of the left fiber end, and its value can be calculated by $1 - R_{L_p}$. These boundary conditions describe the transmission and reflection of light waves at the fiber end. In detail, $P^+(0,\omega,t)$ is the forward-propagating light wave at the left fiber end; $P_{\mathrm{in}}(\omega) T_{L_P}$ is the pump power coupled into the optical fiber and the $R_L(\omega) P^-(0,\omega,t)$ represents the reflected light wave at the left fiber end.

The parameter values set in this simulation are shown in Table 2, in which $\overline{\varepsilon}$ is the average intensity of Rayleigh scattering [3]. Notably, in the simulation, the Rayleigh scattering values are derived from actual experimental data, which are obtained by a phase-sensitive optical time-domain reflectometry (ϕ-OTDR) with proprietary technologies [37].

Figure 3 illustrates the simulation spectra that agree with the characteristics observed in the experimental data. The total spectrum consists of a smooth pedestal and randomly distributed ultra-narrow spikes. This remarkable feature stems from the distinctive feedback mechanism intrinsic to the RRFL [38, 39].

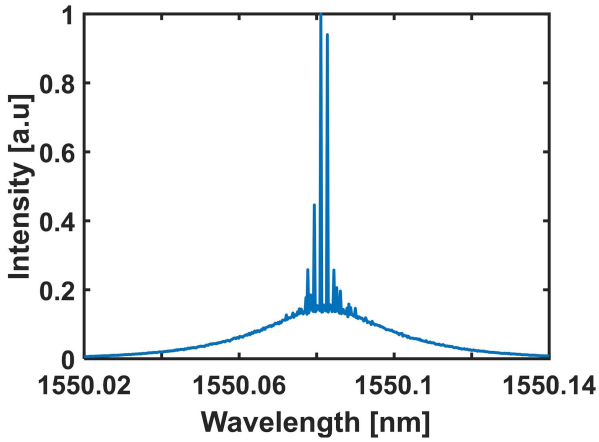

Figure 3 (Color online) Simulation spectrum of random fiber laser based on NLSE model.

3 Results analysis

3.1 Transition state dynamics of RRFL

The generation of random lasers in optical fiber is a rich and intricate process that involves numerous inter-modal interactions and energy transformation dynamics. The correlation map provides detailed information about the specific energy transition dynamics that traditional averaged characterization techniques fail to capture. With the benefit of rapid spectral measurement technique, we can delve deeper into these intrinsic characteristics by calculating the temporal correlations between any two moments and according to

$$\rho(t_1,t_2)=\frac{\langle I(t_1)I(t_2)\rangle-\langle I(t_1)\rangle\langle I(t_2)\rangle}{\sqrt{\langle I^2(t_1)\rangle-\langle I(t_1)\rangle^2}\cdot\sqrt{\langle I^2(t_2)\rangle-\langle I(t_2)\rangle^2}}, \tag{5}$$

where $I(t)$ is the frequency-series array of intensities at any particular moment t obtained from an ensemble of data streams, and the angle brackets represent the ensemble average [40]. $\rho(t_1,t_2)$ represents the relationships between intensity variations of the spectrum at different moments. A correlation matrix is generated when calculating the temporal correlation function, symmetric across the positive diagonal, as shown in Figure 4(a) together with its cross-section. The results give us a clear picture of how various physical processes that influence the evolution of the field at different moments introduce different signatures into the correlation map.

For $\rho=0$, it implies that the spontaneous emission noises are independent of each other. Aside from revealing the noise features, it also provides insights into the physics behind the energy transfer between different spectral traces. The temporal correlation growth curve, depicted in Figure 4(b), illustrates the initial stages of RRFL establishment. The pump energy is mainly transferred to the frequency components at the central wavelength, causing a gradual increase in correlation values. As the RRFL system obtains sufficient energy, the energy variation among different spectral traces decreases, resulting in a deceleration of the correlation's growth rate. This deceleration even causes a slight decrease in the correlation value. Eventually, the correlation remains a stable value, signifying that the RRFL has reached a steady state. It is worth noting that the curve is similar to the Stokes optical power increase curve, following a continuous Verhulst logistic growth curve [31], and this feature is determined by the feedback mechanism of the fiber laser. Figure 4(c) also gives the corresponding simulation results, showing very good agreement with experimental results. There are slight differences between the experimental and simulated results, primarily due to differences in fiber length. However, the fiber length does not affect the correlation evolution laws revealed in this paper, since RRFL systems based on random distributed feedback follow the same excitation mechanism.

However, under the resonant-type feedback mechanism, the growth curve shows notably distinct characteristics. Since the laser is generated from the resonance of the cavity, the temporal correlation follows a step-wise growth pattern, with each step lasting 0.06 ms, corresponding to the cavity round-trip time, as can be seen in the blue curve in Figure 5(a). Furthermore, the output power of the resonant-cavity fiber laser over time can be obtained by integrating individual spectral traces (orange curve). It can

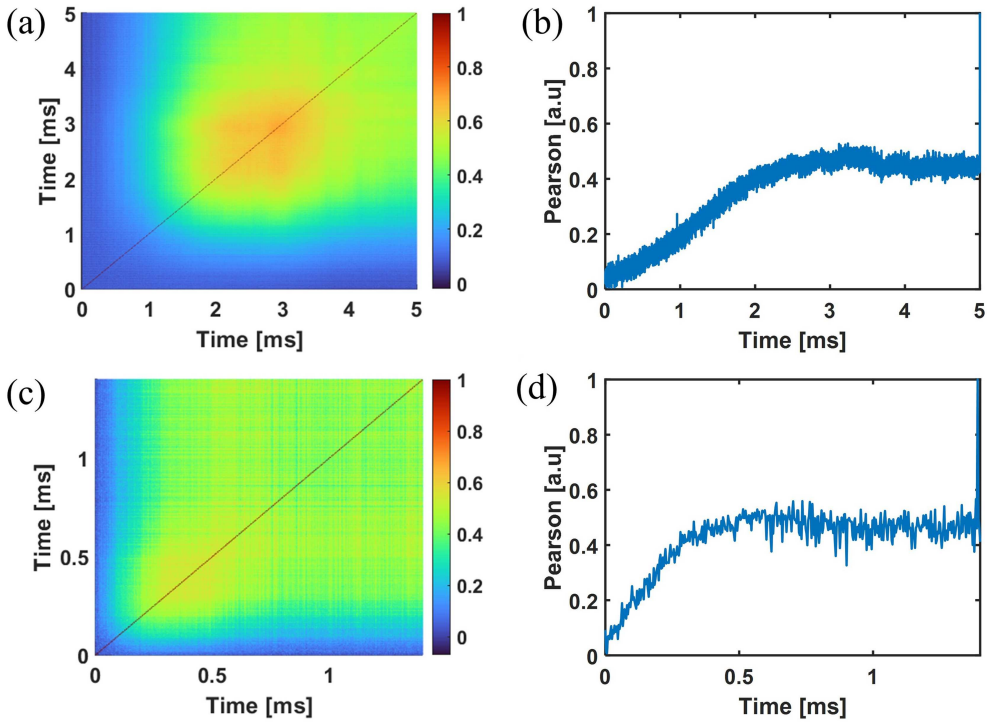

Figure 4 (Color online) Temporal correlation matrix and its cross-section of RRFL in the transitional state. The temporal correlation of RRFL gradually increases, and finally converges to a stable value. (a) and (b) Experiment; (c) and (d) simulation.

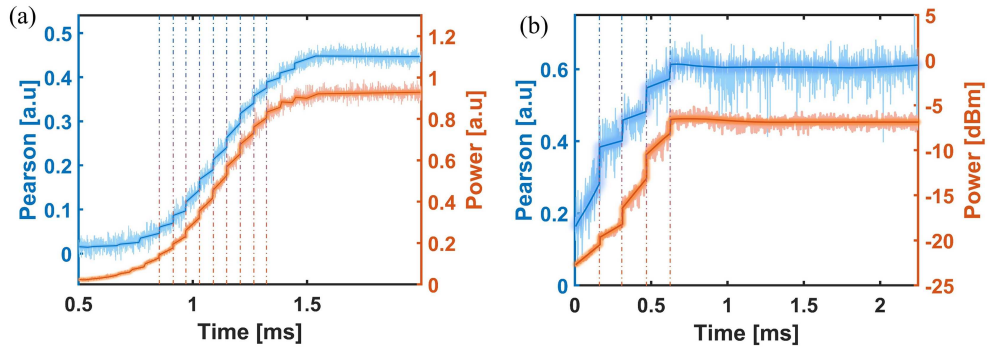

Figure 5 (Color online) Temporal correlation growth curve and power evolution of resonant-cavity fiber laser. The blue curve shows the variation of the Pearson correlation coefficient with RRFL build-up time, and the orange curve represents the evolution of the Stokes optical power. (a) Experiment; (b) simulation.

be seen that under the feedback mechanism of the resonant cavity, the energy transfer of pump light is staged, resulting in a step-like growth curve. The simulation results in Figure 5(b) are in agreement with experimental results. In a word, the growth curve of temporal correlation is influenced by the feedback mechanism and exhibits the same evolution dynamics as the accumulation of intracavity signal optical power.

For a more comprehensive understanding of the governing mechanisms behind the dynamics of spectral evolution and transient characteristics, an analysis was carried out from the perspective of the frequency domain. The spectral correlation $\rho(\lambda_1, \lambda_2)$ between any two wavelengths λ_1 and λ_2 can be obtained according to (5), where $I(\lambda)$ is a time-series array intensity at any specific wavelength λ obtained from an ensemble of the data stream. Calculating $\rho(\lambda_1, \lambda_2)$ yields a correlation matrix, which shows the relationships between intensity variations at different wavelengths. The calculated results are shown in Figure 6, the top row illustrates the experimental results and the bottom row displays the corresponding simulation results. The establishment process of the spectrum is evident: it develops from the center wavelength corresponding to the FBG; as the accumulation of pump energy, the spectrum extends in both the long and short wavelength. Furthermore, the establishment and degradation of spectral correlation

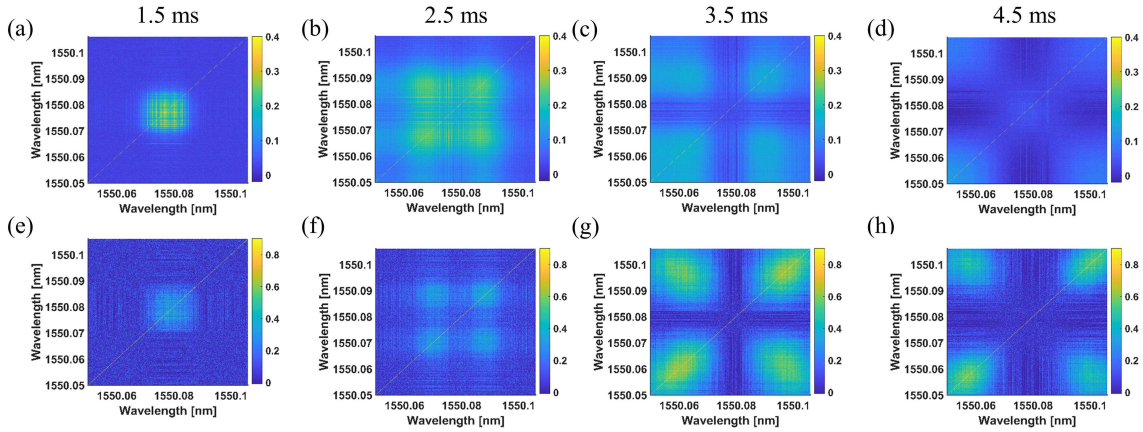

Figure 6 (Color online) Spectral correlation matrices of RRFL in the different moments. (a)–(d) Experimental results; (e)–(h) simulation results. At the early stage of RRFL establishment (before 2.5 ms), the spectral correlation is mainly concentrated at the center wavelength; as the RRFL establishes (after 3.5 ms), the center wavelength spectral correlation gradually degrades, simultaneously, concentrated on both sides of the spectrum.

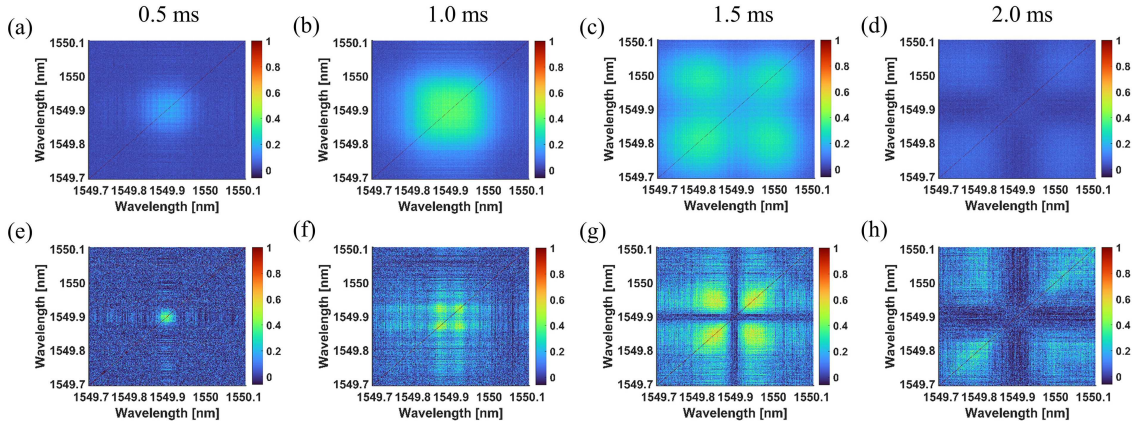

Figure 7 (Color online) Spectral correlation matrices of resonant-cavity fiber laser in the different moments. (a)–(d) Experimental results; (e)–(h) simulation results. At the early stage of laser establishment (before 0.5 ms), the spectral correlation is mainly concentrated at the center wavelength, as the laser establishes (after 1.5 ms), the center wavelength spectral correlation gradually degrades, simultaneously, concentrated on both sides of the spectrum.

in the RRFL transitional states can be observed: the shape of the correlation region transitions from a central-correlated square to a sides-correlated cross.

The physical mechanisms behind this evolution pattern are gain competition and gain sharing between frequency components. Corresponding to the moments in Figure 2(b), in the initial stages of RRFL establishment, due to insufficient pump energy and the wavelength-selective properties of FBG, only the frequency components at the central wavelength acquire sufficient gain for excitation through gain competition. As a result, in the spectral correlation matrix, except for the diagonal and a small square-shaped region around the central wavelength, the correlation of other regions is essentially close to zero. Features of laser generation (positive correlation) continue to develop over time to 2.5 ms, manifesting as an expansion of the square region. However, at 3.5 ms, we observe a degradation of spectral correlation: the map shows a different class of evolution associated with a low-correlation, which is in the form of a blue cross-like structure in the central wavelength. It suggested that the wavelength components determined by the FBG are established, and gain competition and gain sharing among them disappear, resulting in the decrease of correlation. Subsequently, the spectral components on both sides start to establish and show correlation. Figure 7 also depicts the spectral correlation map of the resonant-cavity fiber laser. As expected, the results are consistent with the evolution of RRFL, which reveals the commonality of correlation evolution of laser excitation processes. In the same transitional state, the cross-shaped region with low correlation in a resonant-cavity fiber laser is narrower than that in RRFL, which is attributed to the narrower laser linewidth of the former in the experiment. It is further illustrated that the evolution spectral dynamic revealed in this paper is a universal pattern applicable to spectral generation analysis

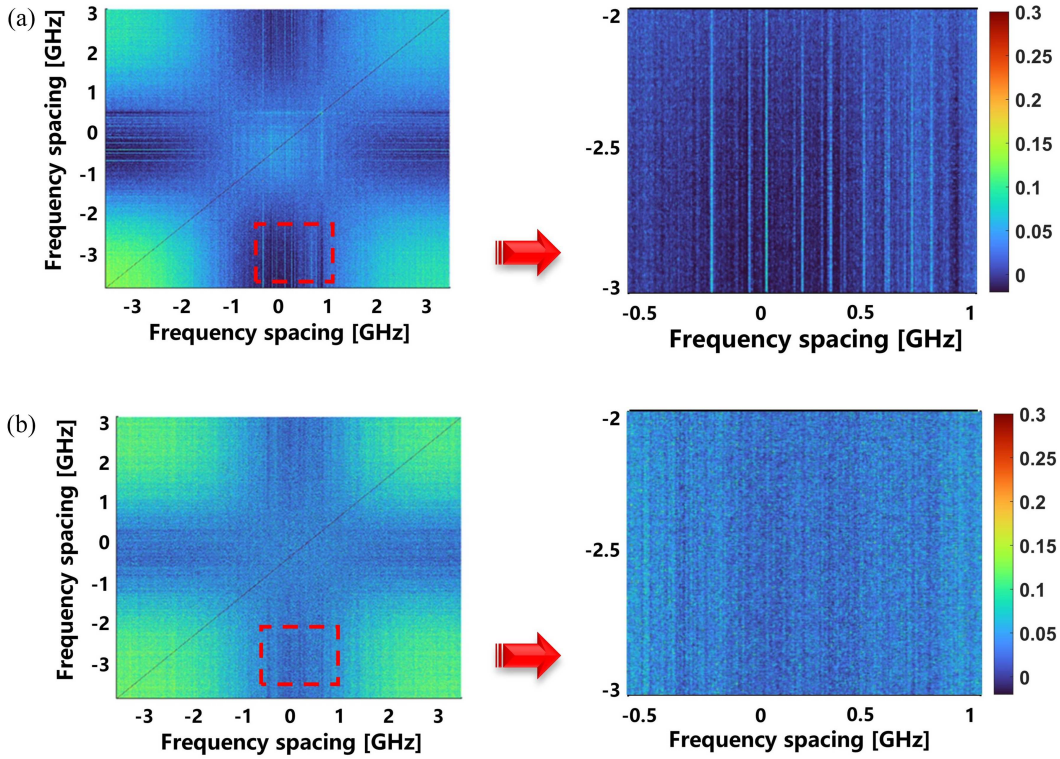

Figure 8 (Color online) Partially correlated features of RRFL in the spectral domain. (a) The temporal correlation of the overall spectrum is shown on the left-hand side, and the corresponding local magnification is shown on the right-hand side. (b) The spectral correlation results of spikes-free RRFL. The frequency spacing is calculated by $\Delta f = f - f_c$ and the f_c is the central frequency.

in fiber lasers employing diverse feedback types.

3.2 Steady state dynamics of RRFL

In addition to the evolutionary characteristics of the RRFL in the transitional states, the microscopic dynamics in the steady states has been investigated comprehensively. It is interesting to observe that the correlation of the RRFL originates from random spikes in the spectra, even though they are only a small proportion of the laser spectrum. This discovery offers a novel method for the precise control of its correlation.

In the spectral domains, when RRFL reaches steady states, the overall spectra exhibit partially correlated features, and the spectral correlation originates from the random spikes. As can be seen in Figure 8(a), the frequency components of the central wavelength show a lower spectral correlation, while the spectral correlation is higher on both sides; the physical mechanism behind this has been analyzed in detail in Subsection 3.1. Notably, in the detail spectrum (the right-hand side of Figure 8(a)), there are many high-correlation random lines near the central wavelength. To further investigate the reasons for the appearance of these high correlation lines, the spikes-free spectra are obtained by increasing the degree of Rayleigh scattering phase fluctuation in optical fibers, where the modes corresponding to the spikes are unable to obtain stable feedback and restrain their excitation. The corresponding spectral correlation results are illustrated in Figure 8(b). Obviously, the high correlation lines disappear after removing the random spikes, indicating that the spectral correlation of RRFL in the steady state is mainly dominated by the random spikes.

According to the feature of partial correlation in the spectral domain, the temporal correlation of the different spectral parts is further investigated, and found that the temporal correlation is also mainly dominated by the random spikes. The whole spectrum of RRFL is divided into three different parts: the central wavelength part, the short-wavelength part, and the long-wavelength part, to explore the temporal correlation properties of local spectra parts. As shown in the middle diagram of Figure 9(a), the temporal correlation is higher in the central wavelength part and lower on both sides parts, contrasting with the case of spectral correlation. Further improving the precision of the spectral subdivision allows

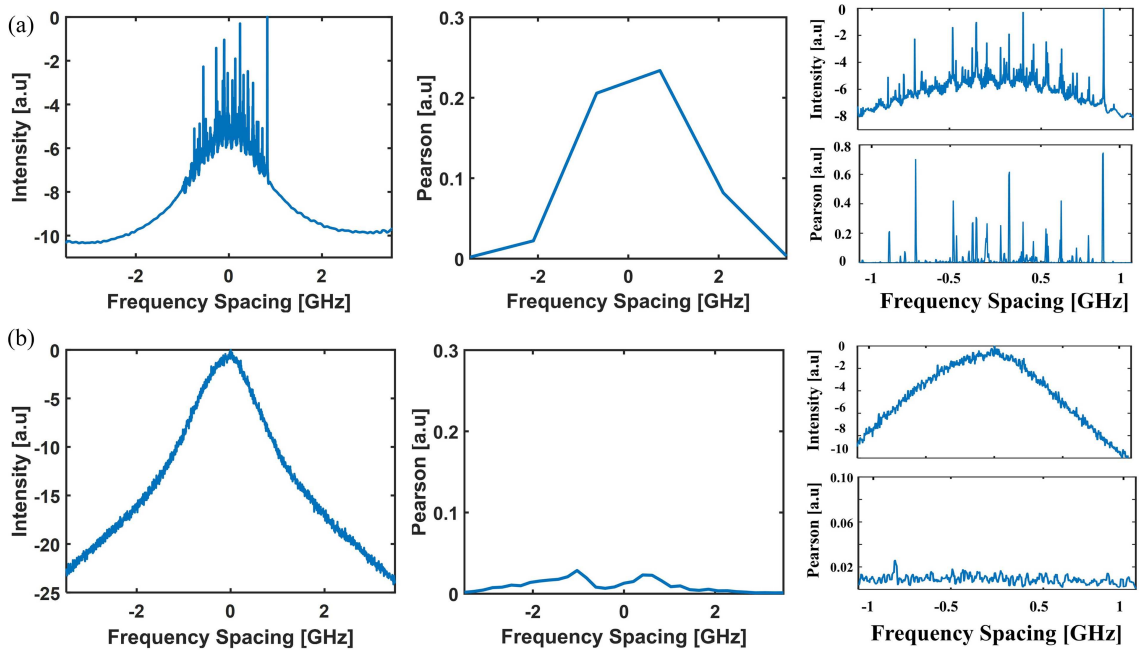

Figure 9 (Color online) Temporal correlation of different spectral parts. (a) Spectra of RRFL and temporal correlation of different spectral parts, and the details of the central wavelength parts with high precision of the spectral subdivision. The high temporal correlation lines correspond to the spectral random spikes one by one. (b) The temporal correlation results of spikes-free RRFL.

for obtaining more details of the temporal correlation and the spectra, as shown in the right-hand side of Figure 9(a). The highly correlated lines in the temporal domain correspond to the random spikes in the RRFL spectrum one by one, indicating that the temporal correlation around the central wavelength in RRFL is mainly attributed to random spikes. To further verify this perspective, the temporal correlation of spikes-free RRFL is also experimentally investigated. The spikes-free spectra are obtained, and the corresponding temporal correlation results are illustrated in Figure 9(b). Unlike the situation with spikes, the central wavelength part exhibits extremely low temporal correlation. This further illustrates that the temporal correlation of the RRFL is mainly dominated by random spikes.

In summary, when RRFL reaches steady states, the overall spectra are partially correlated and its correlation characteristics are dominated by the random spikes. These characteristics are determined by the unique feedback mechanism in RRFL, where coherent feedback can be established in this weakly scattering system, and the interactions between the lasing modes formed by coherent feedback lead to the appearance of high-correlation random spikes. This discovery significantly enriches the theoretical framework of RRFL, contributing to the establishment of a comprehensive theoretical model. Moreover, these unique properties offer multiple means to control the correlation of RRFL. For instance, laser outputs with different correlation degrees can be obtained by filtering different parts of the spectrum; moreover, the number of spikes can be flexibly controlled by rationally designing the system parameters to achieve the RRFL with tunable correlation degrees. Benefiting from its unique correlation characteristics and tunability, the RRFL can be flexibly applied to a wide range of applications such as high-power laser facilities seed source, speckle-free imaging, and temporal ghost imaging [41, 42].

4 Conclusion

In this work, an innovative experimental and theoretical analysis of the temporal-spectral correlation dynamics of RRFL in transitional and steady states is conducted, revealing the interactions between microscopic modes. In the transitional state, due to the unique cavity-free structure of RRFL, the temporal correlation varies continuously and finally converges to a stable value, contrasting with the step-like evolution observed in resonant-cavity lasers. Meanwhile, in the spectral domain, the entire process of formation and degradation of spectral correlation is observed. These findings reveal the commonality in spectral evolution and the differences in temporal evolution between RRFL and resonant-cavity fiber laser. In the steady state, the overall spectra feature partial correlation in the spectral domain and

the temporal-spectral correlation characteristics of RRFL mainly originate from random spikes, which provides novel means for multidimensional control of RRFL. This work provides new insights and methods for exploring the evolution dynamics of broadband continuous lasers. This work fills the crucial research vacancy in the microscopic characteristics of RRFL and greatly enriches the theoretical framework of RRFL, facilitating potential innovative applications in the high-power laser facilities seed source, speckle-free imaging, ultra-long fiber sensing, and optical communications.

Acknowledgements This work was supported by National Natural Science Foundation of China (Grant Nos. 62435002, 62075030), Ministry of Science and Technology of China (Grant No. DL2023167001L), Sichuan Science and Technology Program (Grant No. 2023YFSY0058), and 111 Project (Grant No. B14039).

References

1 Turitsyn S K, Babin S A, El-Taher A E, et al. Random distributed feedback fibre laser. Nat Photon, 2010, 4: 231–235
2 Churkin D V, Sugavanam S, Vatnik I D, et al. Recent advances in fundamentals and applications of random fiber lasers. Adv Opt Photon, 2015, 7: 516–569
3 Qi Y, Ni L, Ye Z, et al. Replica symmetry breaking in 1D Rayleigh scattering system: theory and validations. Light Sci Appl, 2024, 13: 151
4 Han B, Wu H, Liu Y, et al. Ultralong single-ended random fiber laser and sensor. Laser & Photonics Rev, 2023, 17: 2200797
5 Gysel P, Staubli R K. Statistical properties of Rayleigh backscattering in single-mode fibers. J Lightwave Technol, 1990, 8: 561–567
6 Han B, Cheng Q, Tao Y, et al. Spectral manipulations of random fiber lasers: principles, characteristics, and applications. Laser & Photonics Rev, 2024, 18: 2400122
7 Wu H, Wang W, Hu B, et al. Widely tunable continuous-wave visible and mid-infrared light generation based on a dual-wavelength switchable and tunable random Raman fiber laser. Photon Res, 2023, 11: 808
8 de Matos C J S, de Menezes L S, Brito-Silva A M, et al. Random fiber laser. Phys Rev Lett, 2007, 99: 153903
9 Gomes A S L, Moura A L, de Araújo C B, et al. Recent advances and applications of random lasers and random fiber lasers. Prog Quantum Electron, 2021, 78: 100343
10 Chen H, Gao S, Zhang M, et al. Advances in random fiber lasers and their sensing application. Sensors, 2020, 20: 6122
11 Churkin D V, Kolokolov I V, Podivilov E V, et al. Wave kinetics of random fibre lasers. Nat Commun, 2015, 6: 6214
12 Lin S, Wang Z, Li J, et al. Nonlinear dynamics of four-wave mixing, cascaded stimulated Raman scattering and self Q-switching in a common-cavity ytterbium/Raman random fiber laser. Optics Laser Tech, 2021, 134: 106613
13 Wang Z, Wu H, Fan M, et al. High power random fiber laser with short cavity length: theoretical and experimental investigations. IEEE J Sel Top Quantum Electron, 2015, 21: 10–15
14 Pan W, Zhang L, Jiang H, et al. Ultrafast Raman fiber laser with Random distributed feedback. Laser & Photonics Rev, 2018, 12: 1700326
15 Turitsyn S K, Babin S A, Churkin D V, et al. Random distributed feedback fibre lasers. Phys Rep, 2014, 542: 133–193
16 Ma R, Rao Y J, Zhang W L, et al. Multimode random fiber laser for speckle-free imaging. IEEE J Sel Top Quantum Electron, 2019, 25: 1–6
17 Lin S, Wang Z, Qi Y, et al. Wideband remote-sensing based on random fiber laser. J Lightwave Technol, 2022, 40: 3104–3110
18 Fan M, Lin S, Yao K, et al. Spectrum-tailored random fiber laser towards ICF laser facility. Matter Radiat at Extremes, 2023, 8: 025902
19 Churkin D V, Smirnov S V. Numerical modelling of spectral, temporal and statistical properties of Raman fiber lasers. Optics Commun, 2012, 285: 2154–2160
20 Vatnik I D, Gorbunov O A, Sugavanam S, et al. Spatial location of correlations in a random distributed feedback Raman fiber laser. Opt Lett, 2019, 44: 1516
21 Sugavanam S, Sorokina M, Churkin D V. Spectral correlations in a random distributed feedback fibre laser. Nat Commun, 2017, 8: 15514
22 Li J, Wu H, Wang Z, et al. Lévy spectral intensity statistics in a Raman random fiber laser. Opt Lett, 2019, 44: 2799
23 Qi Y, Ni L, Bao X, et al. Experimental evidence of replica symmetry breaking in mode disparities of Raman random fiber laser. In: Proceedings of Conference on Lasers and Electro-Optics, 2024
24 Gomes A S L, Lima B C, Pincheira P I R, et al. Glassy behavior in a one-dimensional continuous-wave erbium-doped random fiber laser. Phys Rev A, 2016, 94: 011801
25 Xia J, Zhang X, Zhou K, et al. Tunable replica symmetry breaking in random laser. Nanophotonics, 2023, 12: 761–771
26 Gorbunov O A, Sugavanam S, Churkin D V. Intensity dynamics and statistical properties of random distributed feedback fiber laser. Opt Lett, 2015, 40: 1783
27 Wu H, Han B, Wang Z, et al. Statistical properties of Er/Yb co-doped random Rayleigh feedback fiber laser. Chin Opt Lett, 2021, 19: 021402
28 Xu J, Wu J, Ye J, et al. Optical rogue wave in random fiber laser. Photon Res, 2020, 8: 1–7
29 Wang X, Xing Y, Chen G, et al. Temporal optical rogue waves in high power short-cavity Yb-doped random fiber laser.

Optics Laser Tech, 2022, 149: 107797

30 González I R R, Lima B C, Pincheira P I R, et al. Turbulence hierarchy in a random fibre laser. Nat Commun, 2017, 8: 15731

31 Lin S T, Wang Z, Zhang J J, et al. Radiation build-up and dissipation in Raman random fiber laser. Sci China Inf Sci, 2024, 67: 112402

32 Coronel E, Das A, González I R R, et al. Evaluation of Pearson correlation coefficient and Parisi parameter of replica symmetry breaking in a hybrid electronically addressable random fiber laser. Opt Express, 2021, 29: 24422

33 Qi Y F, Lin S T, Bao X Y, et al. Random fiber laser dynamic sensing based on rapid spectral detection (in Chinese). Laser Optoelectron Prog, 2023, 60: 1106027

34 Kirik A E, Vatnik I D, Churkin D V. Direct measurements of localized spectral modes in random distributed feedback fiber laser. Results Phys, 2021, 28: 104651

35 Turitsyn S K, Bednyakova A E, Fedoruk M P, et al. Modeling of CW Yb-doped fiber lasers with highly nonlinear cavity dynamics. Opt Express, 2011, 19: 8394

36 Smirnov S V, Churkin D V. Modeling of spectral and statistical properties of a random distributed feedback fiber laser. Opt Express, 2013, 21: 21236

37 Jiang J, Wang Z, Wang Z, et al. Continuous chirped-wave phase-sensitive optical time domain reflectometry. Opt Lett, 2021, 46: 685–688

38 Zhang Y, Wang S, Zheng C, et al. Coherent random fiber laser-enabled super-resolution spectroscopy. ACS Photonics, 2023, 10: 2670–2678

39 Gorbunov O, Vatnik I, Smirnov S, et al. Simulation of narrow generation in a Raman fiber laser with random distributed feedback. Optics Laser Tech, 2024, 174: 110677

40 Schober P, Boer C, Schwarte L A. Correlation coefficients: appropriate use and interpretation. Anesth Analg, 2018, 126: 1763–1768

41 Wu H, Han B, Wang Z, et al. Temporal ghost imaging with random fiber lasers. Opt Express, 2020, 28: 9957–9964

42 Wu H, Hu B, Chen L, et al. Mid-infrared computational temporal ghost imaging. Light Sci Appl, 2024, 13: 124